

Iterative chemical mapping for x-ray spectroscopic ptychography with (incomplete) dictionary

HUIBIN CHANG,^{1,3} PABLO ENFEDAQUE,² STEFANO MARCHESINI^{2,4}

¹ *School of Mathematical Sciences, Tianjin Normal University, Tianjin, China*

² *Computational Research Division, Lawrence Berkeley National Laboratory, Berkeley, CA, USA*

³ *changhuibin@gmail.com*

⁴ *smarchesini@lbl.gov*

Abstract: Spectroscopic ptychography is a powerful technique to determine the chemical composition of a sample with high spatial resolution. In spectro-ptychography a sample is rastered through a focused beam of x-rays with varying photon energy and a series of phaseless diffraction data is recorded. Each chemical component in the material under investigation has a characteristic absorption or phase contrast as a function of photon energy. Using a reference dictionary formed by the set of contrast functions of photon energy of the chemical components, it is possible to obtain the chemical composition of the material from high resolution multi-spectral images. Here we investigate the use of a known or an incomplete dictionary (partially known) in spectroscopic blind-phase retrieval ptychography. We establish a nonlinear spectroscopic ptychography model (SP) model based on Poisson maximum likelihood, and develop fast iterative operator-splitting based algorithms. We show that accurate chemical maps can be recovered even when the scanning stepsizes ($2\times$ FWHM of the probe) are quite large in the case of Poisson noised measurements.

1. Introduction

X-ray spectro-microscopy is a powerful technique to study the chemical and morphological structure of a material at high resolution. The contrast of the material under study in a microscope is recorded as a function of photon energy. The spectral absorption contrast can reveal details about its chemical, orbital or magnetic state [1, 2] of the material intercepted by an x-ray beam.

X-ray ptychography can provide spatial resolution significantly finer than a lens based microscope [3–6] by using phase retrieval of diffraction data recorded to a numerical aperture far larger than is technically feasible to manufacture in x-ray optics. As in standard spectro-microscopy, it is possible to record x-ray ptychography diffraction data at different x-ray photon energies near atomic resonances. Due to the differences for the response of different chemical components to the beam with different energies, the composition map of the sample can be solved based on the measured reference spectra (dictionary). Multi-channel contrasts spectroscopic ptychography is becoming an increasingly popular spectro-microscopy technique [7–12]. The ptychographic reconstruction is normally performed independently for each energy, followed by component analysis [10, 13, 14].

Algorithmically, extensive methods have been developed for the standard ptychography imaging [15–24]. Multi-energy contrasts ptychography [9–11] have been analyzed by applying phase-retrieval analysis independently for different energies, followed by spectral imaging analysis based on known reference spectra or multivariate analysis [25]. More recently, low rank constraint [26] for multi-channel samples was further employed and a gradient descent algorithm with spectral initialization was proposed to recover the higher dimension phase retrieval problem. A hierarchical model with Gaussian-Wishart hierarchical prior was established and a variational expectation-maximization algorithm was further developed [27]. Matrix decomposition based low rank prior [28] was further exploited to reconstruct dynamic, time-varying targets in Fourier

ptychographic imaging.

In this paper, with completely known spectrum or incompletely known spectrum, we will establish an efficient iterative thickness reconstruction method for X-ray ptychography, with unknown probe, within the framework of alternating direction method of multipliers (ADMM) [24, 29] and total variation [30] of the thickness map. Compared with the reconstruction independently for different energies, employing the low-rank structure is expected to improve the reconstruction quality and convergence speed; thickness map could be further improved with the help of total variation regularization. Compared with the two-step method, the proposed joint reconstruction algorithm can generate better results without phase ambiguity, allowing for large scan stepsize. It also has fast convergent with low computation cost for per iteration.

2. Spectroscopic ptychography model (SP) with (incomplete) dictionary

Assuming that L different frequencies of x-rays go through the sample illuminated by the probe ω , one measures phaseless intensities $\{I_l\}_{l=0}^{L-1}$ in the far field, such that with practical Poisson noise occurring for photon-counting, we have

$$I_l = \text{Poi}(|\mathcal{A}(\omega, Y_l)|^2) \text{ for } l = 0, 1, \dots, L-1,$$

with sample contrast maps $Y = (Y_0, Y_1, \dots, Y_{L-1}) \in \mathbb{C}^{N \times L}$, where Poi denotes the Poisson-noise contamination, the bilinear operators $\mathcal{A} : \mathbb{C}^m \times \mathbb{C}^N \rightarrow \mathbb{C}^m$ and $\mathcal{A}_j : \mathbb{C}^m \times \mathbb{C}^N \rightarrow \mathbb{C}^m \forall 0 \leq j \leq L-1$, are denoted as follows: $\mathcal{A}(\omega, u) := (\mathcal{A}_0^T(\omega, u), \mathcal{A}_1^T(\omega, u), \dots, \mathcal{A}_{L-1}^T(\omega, u))^T$, $\mathcal{A}_j(\omega, u) := \mathcal{F}(\omega \circ S_j u)$. Let the spectrum dictionary $D \in \mathbb{C}^{C \times L}$ for different X-rays or its absorption part can be completely measured in advance and the sample be sufficiently thin. Due to C components for different kinds of materials or particles, the sample contrast map can be approximated by first-order Taylor expansion $\exp(XD) \approx \mathbf{1} + XD$ ¹ as

$$Y = \mathbf{1} + XD, \quad (1)$$

given the thickness map of the sample $X = (X_0, X_1, \dots, X_{C-1}) \in \mathbb{R}_+^{N \times C}$.

With the spectrum known completely, in order to determine the thickness map X , one has to solve the following problem

$$\text{To find } X \text{ and } \omega, \text{ s.t. } |\mathcal{A}(\omega, Y_l)|^2 = \text{Poi}(I_l), \quad Y = \mathbf{1} + XD, \quad X \in \mathcal{X}, \quad (2)$$

with non-negative thickness constraint set $\mathcal{X} := \{X \in \mathbb{R}^{N \times C} : X \geq 0\}$. Letting the illumination be normalized, i.e. $\omega \in \mathcal{W} := \{\omega : \|\omega\| = 1\}$, readily we establish the total variation regularized nonlinear optimization model by assuming the piecewise smoothness of the thickness map, which is given below:

$$\text{SP} : \min_{\omega, X, Y} \delta \sum_c \text{TV}(X_c) + \sum_l \mathcal{G}(\mathcal{A}(\omega, Y_l); I_l) + \mathbb{I}_{\mathcal{X}}(X) + \mathbb{I}_{\mathcal{W}}(\omega), \text{ s.t. } Y = \mathbf{1} + XD,$$

where $\mathcal{G}(z, f) := \frac{1}{2} \langle \mathbf{1}, |z|^2 - f \circ \log(|z|^2) \rangle$ derived by the maximum likelihood estimate of Poisson noised data [31].

Experimentally, only the real values part (absorption) of the dictionary D_r are measured, i.e. $\mathcal{D} := \{D : \Re(D) = D_r\}$. As X is real-valued, we consider the following relations as

$$\Re(Y) = D_r X + \mathbf{1}$$

where $D_r := \Re(D)$. Similarly, we derive the following spectroscopic ptychography with incomplete dictionary (SPi) as

$$\text{SPi} : \min_{\omega, X, Y} \delta \sum_c \text{TV}(X_c) + \sum_l \mathcal{G}(\mathcal{A}(\omega, Y_l); I_l) + \mathbb{I}_{\mathcal{X}}(X) + \mathbb{I}_{\mathcal{W}}(\omega), \text{ s.t. } \Re(Y) = \mathbf{1} + D_r X. \quad (3)$$

¹ $\mathbf{1}$ denotes the matrix with all ones elements of the same size of Y and $\exp(\cdot)$ denotes the pointwise exponentiation of the matrix

Remark 2.1. Unlike solving the ptychography imaging independently for each energy, we use the low-rank structure of the recovery results of different energies, i.e. $Y - \mathbf{1}$ has the ranks no more than that of X .

3. Iterative algorithms

ADMM [29] is a powerful and flexible tool which has already been applied to ptychography [19,24] and ptycho-tomography problems [32, 33]. In the following, we will show how to solve the proposed models within the framework of ADMM.

3.1. SP with known dictionary

We show the SP-ADMM algorithm for the proposed SP model, which we refer to as ‘‘SPA’’. Letting $DD^* \in \mathbb{C}^{C \times C}$ be non-singular, for the constraint in (1), one can get an equivalent form as

$$X = (Y - \mathbf{1})\hat{D} \quad (4)$$

with $\hat{D} := D^*(DD^*)^{-1} \in \mathbb{C}^{L \times C}$. Thus, we consider the following equivalent model by further introducing auxiliary variables $\{Z_l\}$:

$$\begin{aligned} \min_{\omega, X, Y} \quad & \delta \sum_c \text{TV}(X_c) + \sum_l \mathcal{G}(Z_l; I_l) + \mathbb{I}_{\mathcal{X}}(X) + \mathbb{I}_{\mathcal{Y}}(\omega), \\ \text{s.t.} \quad & Z_l = \mathcal{A}(\omega, Y_l), X = (Y - \mathbf{1})\hat{D} \quad \forall 0 \leq l \leq L - 1. \end{aligned} \quad (5)$$

One will see the benefit by considering (4) instead of (1) as (i) the multiplier will be a low-dimensional variable since the dimension of Y is much higher than that of X ; (ii) The subproblem w.r.t. the variable X can be more easily solved.

An equivalent saddle point problem for (5) based on the augmented Lagrangian is derived below:

$$\begin{aligned} \max_{\Lambda, \Gamma} \min_{\omega, X, Y, Z} \quad & \mathcal{L}_{\lambda, \beta}(\omega, X, Y, Z, \Lambda, \Gamma) \\ := & \delta \sum_c \text{TV}(X_c) + \sum_l \mathcal{G}(Z_l; I_l) + \mathbb{I}_{\mathcal{X}}(X) + \mathbb{I}_{\mathcal{Y}}(\omega), \\ & + \sum_l (\lambda \Re \langle Z_l - \mathcal{A}(\omega, Y_l), \Lambda_l \rangle + \frac{\lambda}{2} \|Z_l - \mathcal{A}(\omega, Y_l)\|^2) \\ & + \beta \Re \langle X - (Y - \mathbf{1})\hat{D}, \Gamma \rangle + \frac{\beta}{2} \|X - (Y - \mathbf{1})\hat{D}\|^2, \end{aligned}$$

with the multipliers $\Lambda := (\Lambda_0, \dots, \Lambda_{L-1})$ and Γ , where $\langle \cdot, \cdot \rangle$ denotes the inner product of vectors and for matrices (trace norms) respectively.

The above saddle point problem can be solved by alternating minimization and update of multipliers. We first focus on each sub-minimization problems. For the ω -subproblem, with the additional proximal term, we have

$$\begin{aligned} \omega^* & := \arg \min_{\omega} \mathcal{L}_{\lambda, \beta}(\omega, X, Y, Z, \Lambda, \Gamma) \\ & = \arg \min_{\omega} \frac{1}{2} \sum_l \|Z_l + \Lambda_l - \mathcal{A}(\omega, Y_l)\|^2 + \mathbb{I}_{\mathcal{Y}}(\omega) \\ & = \arg \min_{\omega \in \mathcal{Y}} \frac{1}{2} \sum_{l,j} \|\mathcal{F}^*(Z_{l,j} + \Lambda_{l,j}) - \omega \circ \mathcal{S}_j Y_l\|^2. \end{aligned}$$

The first-order gradient of the above least squares problem (without constraint) is given below

$$\text{diag}(\sum_{l,j} |\mathcal{S}_j Y_l|^2) \omega - \sum_{l,j} \mathcal{F}^*(Z_{l,j} + \Lambda_{l,j}) \circ \mathcal{S}_j Y_l^*.$$

Immediately, one gets the projected gradient descent scheme with preconditioning as

$$\begin{aligned} \omega_{s+1} & = \text{Proj}_{\mathcal{X}} \left(\omega_s - \frac{\text{diag}(\sum_{l,j} |\mathcal{S}_j Y_l|^2) \omega_s - \sum_{l,j} \mathcal{F}^*(Z_{l,j} + \Lambda_{l,j}) \circ \mathcal{S}_j Y_l^*}{(\sum_{l,j} |\mathcal{S}_j Y_l|^2) + \gamma_1 \mathbf{1}} \right) \\ & = \text{Proj}_{\mathcal{X}} \left(\frac{\gamma_1 \omega_s}{(\sum_{l,j} |\mathcal{S}_j Y_l|^2) + \gamma_1 \mathbf{1}} + \frac{\sum_{l,j} \mathcal{F}^*(Z_{l,j} + \Lambda_{l,j}) \circ \mathcal{S}_j Y_l^*}{(\sum_{l,j} |\mathcal{S}_j Y_l|^2) + \gamma_1 \mathbf{1}} \right) \quad s = 0, 1, \dots \end{aligned} \quad (6)$$

with the parameter $\gamma_1 > 0$ and $\text{Proj}_{\mathcal{W}}(\omega) := \frac{\omega}{\|\omega\|}$.

For the X -subproblem, one has

$$\begin{aligned} X^* &:= \arg \min_X \mathcal{L}_{\lambda, \beta}(\omega, X, Y, Z, \Lambda, \Gamma) \\ &= \arg \min_X \sum_c \left(\frac{\delta}{\beta} \text{TV}(X_c) + \frac{1}{2} \|X_c - \mathfrak{R}((Y - \mathbf{1})\hat{D} - \Gamma)_c\|^2 \right) + \mathbb{I}_{\mathcal{X}}(X). \end{aligned}$$

Since it is quite standard to solve the total variation denoising problem by using first order operator-splitting algorithm [34, 35], we directly give the solution below:

$$X_c^* = \max\{0, \text{Denoise}_{\delta/\beta}(\mathfrak{R}((Y - \mathbf{1})\hat{D} - \Gamma)_c)\} \quad \forall 0 \leq c \leq C - 1,$$

with $\text{Denoise}_\nu(u_0) := \arg \min_u \nu \text{TV}(u) + \frac{1}{2} \|u - u_0\|^2$.

For the Y -subproblem, with additional proximal term $\frac{\gamma_2}{2} \|Y - Y_0\|^2$ and previous iterative solution Y^0 , one has

$$\begin{aligned} Y^* &:= \arg \min_Y \mathcal{L}_{\lambda, \beta}(\omega, X, Y, Z, \Lambda, \Gamma) \\ &= \arg \min_Y \frac{\lambda}{2} \sum_l \|\mathcal{A}(\omega, Y_l) - (\Lambda_l + Z_l)\|^2 + \frac{\beta}{2} \|Y\hat{D} - (\Gamma + X + \mathbf{1}\hat{D})\|^2 + \frac{\gamma_2}{2} \|Y - Y_0\|^2 \\ &= \arg \min_Y \frac{\lambda}{2} \sum_l \|\omega \circ \mathcal{S}_j Y_l - \mathcal{F}^*(\Lambda_l + Z_l)\|^2 + \frac{\beta}{2} \|Y\hat{D} - (\Gamma + X + \mathbf{1}\hat{D})\|^2 + \frac{\gamma_2}{2} \|Y - Y_0\|^2 \\ &= \arg \min_Y \frac{\lambda}{2} \sum_l \|\mathcal{S}_j^T \omega \circ Y_l - \mathcal{S}_j^T \mathcal{F}^*(\Lambda_l + Z_l)\|^2 + \frac{\beta}{2} \|Y\hat{D} - (\Gamma + X + \mathbf{1}\hat{D})\|^2 + \frac{\gamma_2}{2} \|Y - Y_0\|^2. \end{aligned}$$

By calculating the first-order gradient of the above least squares problem, one has

$$\text{diag}(\lambda \sum_j |\mathcal{S}_j^T \omega|^2 + \gamma_2 \mathbf{I})Y + \beta Y \hat{D} \hat{D}^* = \lambda Q + \gamma_2 Y_0 + \beta(\Gamma + X + \mathbf{1}\hat{D})\hat{D}^*,$$

where $Q := (Q_0, Q_1, \dots, Q_{L-1}) \in \mathbb{C}^{N, L}$ with $Q_l := \sum_j \mathcal{S}_j^T (\omega^* \circ \mathcal{F}^*(\Lambda_l + Z_l))$, which is actually the Sylvester equation. Assume that the positive Hermitian $\hat{D}\hat{D}^*$ has the singular-value-decomposition (SVD) as $\hat{D}\hat{D}^* = V\mathcal{S}V^*$, with diagonal matrix (diagonal elements are singular values) $\mathcal{S} \in \mathbb{R}^{L \times L}$ and unitary matrix $V \in \mathbb{C}^{L \times L}$. Therefore, by introducing $\hat{Y} := YV$, one has

$$\text{diag}(\lambda \sum_j |\mathcal{S}_j^T \omega|^2 + \gamma_2 \mathbf{I})\hat{Y} + \beta \hat{Y} \mathcal{S} = (\lambda Q + \gamma_2 Y_0 + \beta(\Gamma + X + \mathbf{1}\hat{D})\hat{D}^*)V,$$

with identity operator \mathbf{I} , such that the closed form solution can be given below:

$$Y^* = \hat{Y}^* V^*, \quad (7)$$

where $\hat{Y}^* := (\hat{Y}_0^*, \dots, \hat{Y}_{L-1}^*) \in \mathbb{C}^{N \times L}$, and

$$\hat{Y}_l^* = \frac{((\lambda Q + \gamma_2 Y_0 + \beta(\Gamma + X + \mathbf{1}\hat{D})\hat{D}^*)V)_l}{(\lambda \sum_j |\mathcal{S}_j^T \omega|^2 + \gamma_2 \mathbf{1}) + \beta \mathcal{S}_{l,l} \mathbf{1}} \quad \forall 0 \leq l \leq L - 1. \quad (8)$$

For the Z -subproblem, we have [31]

$$Z^* := \arg \min_Z \sum_l \mathcal{G}(Z_l; I_l) + \frac{\lambda}{2} \sum_l \|Z_l - (\mathcal{A}(\omega, Y_l) - \Lambda_l)\|^2,$$

that gives

$$Z_l^* = \frac{\sqrt{4(1+\lambda)I_l + \lambda^2 |\hat{Z}_l|^2 + \lambda |\hat{Z}_l|}}{2(1+\lambda)} \circ \text{sign}(\hat{Z}_l),$$

with $\hat{Z}_l := \mathcal{A}(\omega, Y_l) - \Lambda_l$. Based on the above calculations and the update of multipliers, the overall algorithm can be summarized below:

Algorithm 1: SP-ADMM (SPA)

0. Initialization: Compute the SVD of $\hat{D}\hat{D}^*$ as $\hat{D}\hat{D}^* = V\mathcal{S}V^*$. Set $Y^0 := \mathbf{1}, \omega^0 := \mathcal{F}^* \left(\frac{\sum_{l,j} \sqrt{I_{l,j}}}{L \times J} \right), Z_l^0 := \mathcal{A}(\omega^0, Y_l^0), \Lambda = \mathbf{0}$, and $\Gamma = \mathbf{0}$. Set $k := 0$.

1. Update the probe ω^{k+1} by one-step projected gradient descent method

$$\omega^{k+1} = \text{Proj}_{\mathcal{X}} \left(\frac{\gamma_1 \omega^k}{(\sum_{l,j} |\mathcal{S}_j Y_l^k|^2) + \gamma_1 \mathbf{1}} + \frac{\sum_{l,j} \mathcal{F}^*(Z_{l,j}^k + \Lambda_{l,j}^k) \circ \mathcal{S}_j (Y_l^k)^*}{(\sum_{l,j} |\mathcal{S}_j Y_l^k|^2) + \gamma_1 \mathbf{1}} \right), \quad (9)$$

with $\gamma_1 = 1.0 \times 10^{-3} \times \|\sum_{l,j} |\mathcal{S}_j Y_l^k|^2\|_{\infty}$.

2. Update the thickness function X^{k+1} by

$$X_c^{k+1} = \max\{0, \text{Denoise}_{\delta/\beta}(\mathfrak{X}(((Y^k - \mathbf{1})\hat{D} - \Gamma^k))_c)\} \quad \forall 0 \leq c \leq C - 1.$$

3. Update Y^{k+1} by

$$Y^{k+1} = \hat{Y}^{k+1} V^*, \quad \hat{Y}_l^{k+1} = \frac{((\lambda Q^k + \gamma_2^k Y^k + \beta(\Gamma^k + X^{k+1} + \mathbf{1}\hat{D})\hat{D}^*)V)_l}{(\lambda \sum_j |\mathcal{S}_j^T \omega^{k+1}|^2 + \gamma_2^k \mathbf{1}) + \beta \mathcal{S}_{l,l} \mathbf{1}} \quad \forall 0 \leq l \leq L - 1. \quad (10)$$

with $Q^k := (Q_0^k, Q_1^k, \dots, Q_{L-1}^k) \in \mathbb{C}^{N,L}$, $Q_l^k := \sum_j \mathcal{S}_j^T ((\omega^{k+1})^* \circ \mathcal{F}^*(\Lambda_l^k + Z_l^k))$, and $\gamma_2^k = 1.0 \times 10^{-3} \times \lambda \|\sum_j |\mathcal{S}_j \omega^{k+1}|^2\|_{\infty}$.

4. Update the auxiliary variable Z^{k+1} by

$$Z_l^{k+1} = \frac{\sqrt{4(1+\lambda)I_l + \lambda^2 |\hat{Z}_l^k|^2 + \lambda |\hat{Z}_l^k|}}{2(1+\lambda)} \circ \text{sign}(\hat{Z}_l^k),$$

with $\hat{Z}_l^k := \mathcal{A}(\omega^{k+1}, Y_l^{k+1}) - \Lambda_l^k$.

5. Update the multipliers Λ and Γ by

$$\begin{aligned} \Lambda_l &\leftarrow \Lambda_l + Z_l - \mathcal{A}(\omega, \mathcal{T}_l Y_l) \quad \forall 0 \leq l \leq L - 1; \\ \Gamma &\leftarrow \Gamma + X - (Y - \mathbf{1})\hat{D}. \end{aligned}$$

6. If satisfying the stopping condition, then output X^{k+1} as the final thickness; Otherwise, go to Step 1.

3.2. SP with incomplete dictionary

By further assuming that D_r has full row-rank, i.e. $D_r D_r^*$ is non-singular, with known $\hat{D}_r := D_r^T (D_r D_r^T)^{-1}$ in advance, one readily has:

$$X = \mathfrak{X}(Y - \mathbf{1})\hat{D}_r.$$

One readily has to solve the following equivalent problem instead of (3):

$$\min_{\omega, X, Y} \delta \sum_c \text{TV}(X_c) + \sum_l \mathcal{G}(\mathcal{A}(\omega, Y_l); I_l) + \mathbb{I}_{\mathcal{X}}(X) + \mathbb{I}_{\mathcal{W}}(\omega), \quad \text{s.t. } X = \mathfrak{X}(Y - \mathbf{1})\hat{D}_r. \quad (11)$$

Similarly to the previous subsection, introducing the multiplier Γ_r and auxiliary variable Z yields the saddle point problem gives below, with the help of the augmented Lagrangian of (11):

$$\begin{aligned} \max_{\Lambda, \Gamma_r} \min_{\omega, X, Y, Z} \widetilde{\mathcal{L}}_{\lambda, \beta}(\omega, X, Y, Z, \Lambda, \Gamma_r) &:= \delta \sum_c \text{TV}(X_c) + \sum_l \mathcal{G}(Z_l; I_l) + \mathbb{I}_{\mathcal{X}}(X) + \mathbb{I}_{\mathcal{Y}}(\omega) \\ &+ \sum_l \left(\lambda \Re \langle Z_l - \mathcal{A}(\omega, Y_l), \Lambda_l \rangle + \frac{\lambda}{2} \|Z_l - \mathcal{A}(\omega, Y_l)\|^2 \right) \\ &+ \beta \langle X - \Re(Y - \mathbf{1}) \hat{D}_r, \Gamma_r \rangle + \frac{\beta}{2} \|X - \Re(Y - \mathbf{1}) \hat{D}_r\|^2. \end{aligned}$$

We only focus on the differences compared with SPA. For the X -subproblem, we have

$$X^* := \arg \min \frac{\delta}{\beta} \sum_c \text{TV}(X_c) + \mathbb{I}_{\mathcal{X}}(X) + \frac{1}{2} \|X - (\Re(Y - \mathbf{1}) \hat{D}_r - \Gamma_r)\|^2.$$

Hence we get

$$X_c^* = \max\{0, \text{Denoise}_{\delta/\beta}((\Re(Y - \mathbf{1}) \hat{D}_r - \Gamma_r)_c)\} \quad \forall 0 \leq c \leq C - 1.$$

For the Y -subproblem with proximal terms $\|Y - Y_0\|^2$, we have

$$Y^* := \arg \min_Y \frac{\lambda}{2} \sum_{j,l} \|S_j^T \omega \circ Y_l - S_j^T \mathcal{F}^*(\Lambda_l + Z_l)\|^2 + \frac{\beta}{2} \|X - \Re(Y - \mathbf{1}) \hat{D}_r + \Gamma_r\|^2 + \frac{\hat{\gamma}_2}{2} \|Y - Y_0\|^2,$$

that results in the following equations w.r.t. the real and imaginary parts respectively:

$$\begin{cases} \text{diag}(\lambda \sum_j |S_j^T \omega|^2 + \hat{\gamma}_2 \mathbf{1}) \Re(Y) + \beta \Re(Y) \hat{D}_r \hat{D}_r^T = \lambda \Re(Q) + \hat{\gamma}_2 \Re(Y_0) + \beta(\Gamma_r + X + \mathbf{1} \hat{D}_r) \hat{D}_r^T \\ \text{diag}(\lambda \sum_j |S_j^T \omega|^2 + \hat{\gamma}_2 \mathbf{1}) \Im(Y) = \lambda \Im(Q) + \hat{\gamma}_2 \Im(Y_0). \end{cases}$$

Then one can solve the real part of Y by (7)-(8), while the imaginary part can be simply computed by

$$\Im(Y) = \frac{\lambda \Im(Q) + \hat{\gamma}_2 \Im(Y_0)}{\lambda \sum_j |S_j^T \omega|^2 + \hat{\gamma}_2 \mathbf{1}}.$$

We summarize the overall SPi-ADMM algorithm (“i” means the incomplete dictionary) below:

Algorithm 2: SPi-ADMM (SPiA)

0. Initialization: Compute the SVD of $\hat{D}_r \hat{D}_r^*$ as $\hat{D}_r \hat{D}_r^* = V_r \mathcal{S}_r V_r^*$. Set $Y^0 := \mathbf{1}, \omega^0 := \mathcal{F}^* \left(\frac{\sum_{l,j} \sqrt{I_{l,j}}}{L \times J} \right), Z_l^0 := \mathcal{A}(\omega^0, Y_l^0), \Lambda = \mathbf{0}$, and $\Gamma_r = \mathbf{0}$. Set $k := 0$.

1. Update the probe ω^{k+1} as Step 1 of Algorithm 1 (SPA).

2. Update the thickness function X^{k+1} by

$$X_c^{k+1} = \max\{0, \text{Denoise}_{\delta/\beta}((\Re(Y^k - \mathbf{1}) \hat{D}_r - \Gamma_r^k)_c)\} \quad \forall 0 \leq c \leq C - 1.$$

3. Update $Y^{k+1} = Y_r^{k+1} + i \times Y_i^{k+1}$ (Imaginary unit $i := \sqrt{-1}$) with real part update by

$$Y_r^{k+1} = \hat{Y}_r^{k+1} V_r^*, \quad (\hat{Y}_r^{k+1})_l = \frac{((\lambda \Re(Q^k) + \hat{\gamma}_2 \Re(Y^k) + \beta(\Gamma_r^k + X^{k+1} + \mathbf{1} \hat{D}_r) \hat{D}_r^*) V)_l}{(\lambda \sum_j |S_j^T \omega^{k+1}|^2 + \hat{\gamma}_2 \mathbf{1}) + \beta \mathcal{S}_{l,l} \mathbf{1}} \quad \forall 0 \leq l \leq L-1, \quad (12)$$

with $\hat{\gamma}_2^k = 1.0 \times 10^{-3} \times \lambda \|\sum_j |S_j \omega^{k+1}|^2\|_\infty$, and imaginary part update by

$$Y_i^{k+1} = \frac{\lambda \Im(Q^k) + \hat{\gamma}_2 \Im(Y^k)}{\lambda \sum_j |S_j^T \omega^{k+1}|^2 + \hat{\gamma}_2 \mathbf{1}}.$$

4. Update the auxiliary variable Z^{k+1} as Step 4 of Algorithm 1 (SPA).
5. Update the multipliers Λ and Γ_r by

$$\begin{aligned}\Lambda_l &\leftarrow \Lambda_l + Z_l - \mathcal{A}(\omega, \mathcal{T}Y_l) \forall 0 \leq l \leq L - 1; \\ \Gamma_r &\leftarrow \Gamma_r + X - \Re(Y - \mathbf{1})\hat{D}_r.\end{aligned}$$

6. If satisfying the stopping condition, then output X^{k+1} as the final thickness; Otherwise, go to Step 1.

4. Simulations

For this experimental analysis, we consider synthetic thickness maps of three different materials, extracted from three channels (RGB) of a natural color image (after thresholding and shift, 256×256 pixels), shown in Fig. 1. The real part of the spectrum dictionary (the spectrum of two different materials -PMMA and PS - plus a constant w.r.t. ten different energies) was measured at the Advanced Light Source [36] and the imaginary part was derived using Kramers-Kronig relations [37] and are shown in Fig. 2.

The ptychography measurements are simulated with Poisson noise contamination, using a single grid scan with non-periodical boundary at each energy, where a standard zone-plate (with 64 pixels on the detector) is used for the probe with beam width (FWHM) of 16 pixels.

In order to evaluate the recovery results, the signal-to-noise ratio (SNR) (The larger, the better) is used, which is denoted below:

$$\text{SNR}(X, X_g) = -10 \log_{10} \|X - X_g\|^2 / \|X\|^2, \quad (13)$$

where X_g corresponds to the ground truth thickness.

We compare the proposed algorithms SPA and SPiA with a two-step method (First do ptychography with joint illumination, and then do spectroscopy with known dictionary (or only real part) and correction of phase ambiguity for different energies).

We also show the performance of proposed algorithms without regularization, where we simply set the regularization parameter $\delta = 0$ and slightly adjust the algorithms by replacing Step 2 with

$$X^{k+1} = \max\{0, \Re((Y^k - \mathbf{1})\hat{D} - \Gamma^k)\}, \quad (14)$$

for SPA and

$$X^{k+1} = \max\{0, \Re(Y^k - \mathbf{1})\hat{D}_r - \Gamma_r^k\}. \quad (15)$$

4.1. Performances of SPA and SPiA

With scan stepsize 32 pixels, we show the recovered results by proposed algorithms, compared with the two-step method, and please see Fig. 3 for the case with complete dictionary, and Fig. 4 for the case of incomplete dictionary. Visually, one can readily see that there are obvious artifacts in the recovered thickness by two-step method as shown in the first row of Figs. 3-4, while much less artifacts are visible in the second and third rows and of Figs. 3-4 by proposed SPA. Namely, one can see the improvements in the region located at the red and blue circles of the results. Furthermore, the SNRs of the recovery results by the two-step methods and proposed SPA are 14.0, 17.9 (no regularization with $\delta = 0$), and 18.6, and one can readily see the gain by the proposed algorithms. For the case of only knowing the real part of the dictionary, the SNRs by the two-step method and proposed SPiA are 13.8, 15.8, and 16.7, where similarly at least 2dB increase is gained by proposed algorithms.

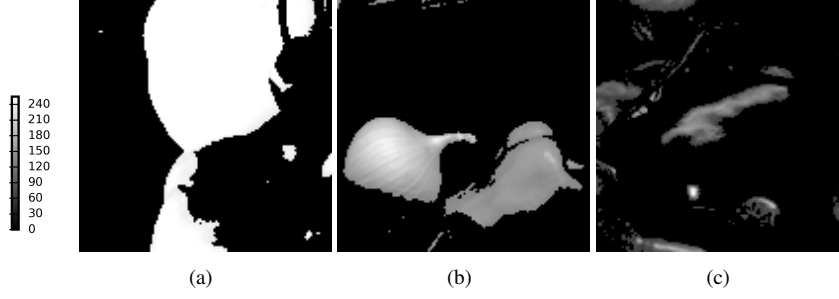


Fig. 1. (a)-(c) Truth for three different materials

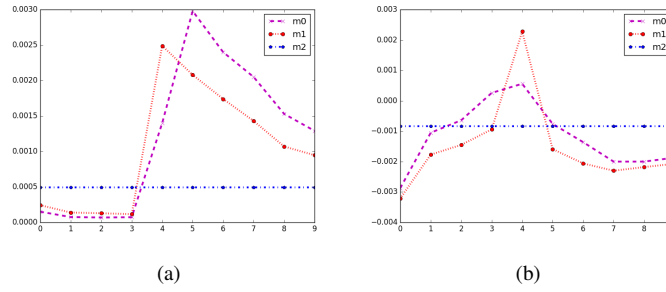


Fig. 2. Spectrum dictionaries (three different materials m_0 , m_1 and m_2) with real part in (a) and imaginary part in (b). The x-axis, and y-axis denotes the spectrum, and different energies respectively.

The phase ambiguity led to less accuracy, and therefore it is quite important to correct the phase ambiguity for a two-step method. For example, for the test shown in Fig. 3, the SNR without phase correction is only 12.3, while reaches 14.0 after correction. However, our proposed algorithm seems more efficient, since there is no need to correct the phase ambiguity due to the iterative reconstruction employing the low-rank structure and positivity constraint of thickness function.

4.2. Different scan stepsizes

We test the robustness of proposed algorithms w.r.t. different scan stepsizes. We report the quantitative results in Table 1, where the obvious increase of SNRs can be readily observed. Especially we show the recovery results with stepsize 40 pixels in Fig. 5, and one can see the dramatic improvement by the proposed method. Namely for the features within the blue and red circles in Fig. 5 are almost lost by the two-step method, while can be clearly observed by proposed method.

4.3. Convergence

We show the error changes of proposed algorithm in Fig. 6, where one can observe the steady decrease of the successive errors of proposed algorithm.

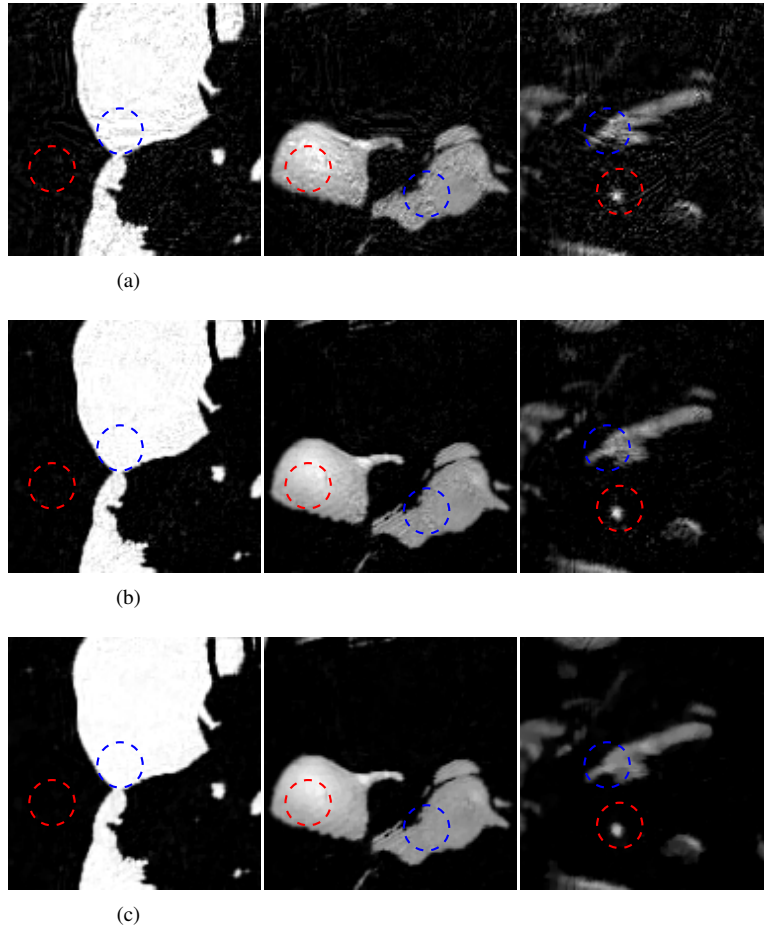


Fig. 3. Performances (Poisson noisy data with $\text{SNR}=29.2$ with scan stepsize=32) of SPA: (a)-(c): Recovery results by a two-step method; (d)-(f): Recovery results by proposed SPA without regularization; (g)-(i) proposed SPA

5. Conclusions

In this paper, we have proposed the SPA and SPiA algorithms to determine the thickness map for spectroscopic ptychography imaging. Numerical experiments show that the proposed algorithms are able to produce more accurate results with clearer features, and fast convergence, compared with the two-step method. In the future, we will extend our work to the thick sample, where the first-order Taylor expansion is not sufficiently accurate and the case with completely unknown dictionary, investigate the use of Kramers-Kronig relationships [38], and further provide software for real experimental data analysis.

6. Acknowledgments

This work of the first author was partially supported by National Natural Science Foundation of China (Nos.11871372, 11501413), Natural Science Foundation of Tianjin (No.18JCYBJC16600), 2017-Outstanding Young Innovation Team Cultivation Program (No.043-135202TD1703) and Innovation Project (No.043-135202XC1605) of Tianjin Normal University, Tianjin Young

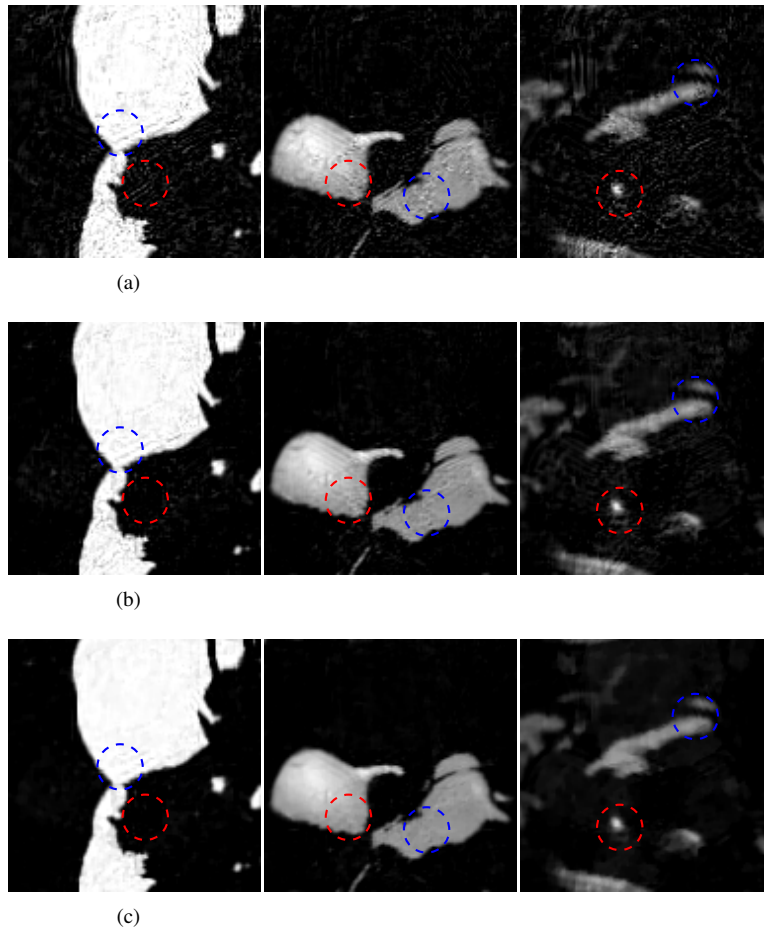


Fig. 4. Performances (Poisson noisy data with SNR=29.2 with scan stepsize=32) of SPiA: (a)-(c): Recovery results by a two-step method; (d)-(f): Recovery results by proposed SPiA without regularization; (g)-(i) proposed SPiA

Backbone of Innovative Personnel Training Program and Program for Innovative Research Team in Universities of Tianjin (No.TD13-5078). This work was partially funded by the Advanced Light Source and the Center for Advanced Mathematics for Energy Research Applications, a joint ASCR-BES funded project within the Office of Science, US Department of Energy, under contract number DOE-DE-AC03-76SF00098.

References

1. J. Stöhr, *NEXAFS spectroscopy*, vol. 25 (Springer Science & Business Media, 2013).
2. D. Koningsberger and R. Prins, *X-ray absorption : principles, applications, techniques of EXAFS, SEXAFS and XANES*, Chemical analysis (Wiley-Interscience, 1988).
3. P. Nellist, B. McCallum, and J. Rodenburg, "Resolution beyond the 'information limit' in transmission electron microscopy," *Nature* **374**, 630 (1995).
4. H. N. Chapman, "Phase-retrieval x-ray microscopy by wigner-distribution deconvolution," *Ultramicroscopy* **66**, 153–172 (1996).
5. J. M. Rodenburg and H. M. Faulkner, "A phase retrieval algorithm for shifting illumination," *Appl. physics letters* **85**, 4795–4797 (2004).

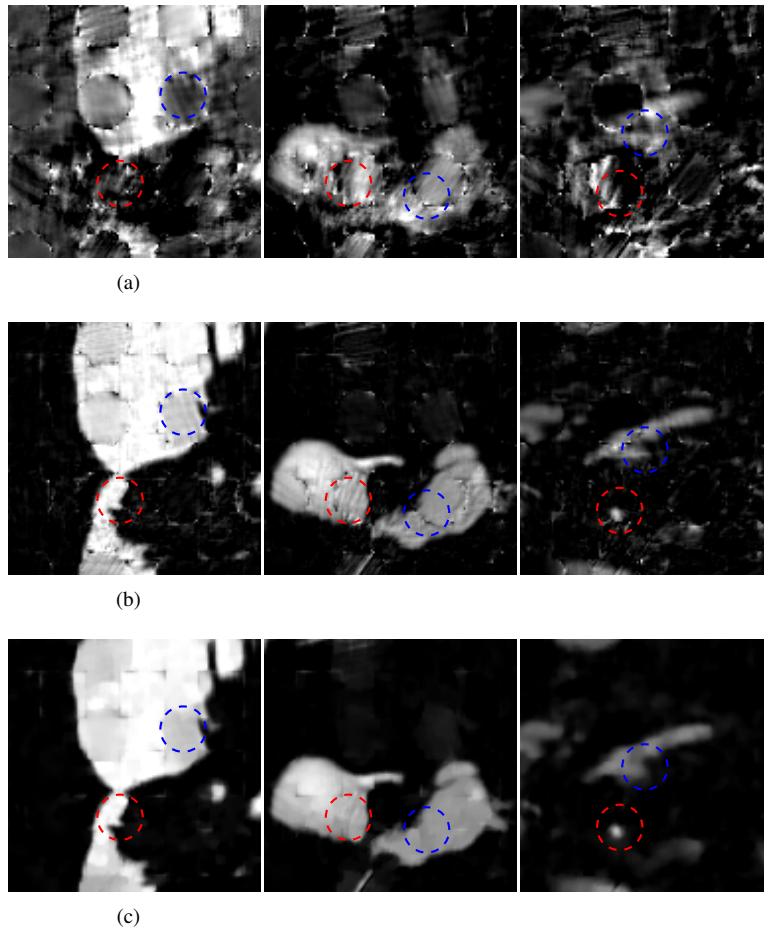


Fig. 5. Performances (Poisson noisy data with SNR=29.2 with scan stepsize=40): (a)-(c): Recovery results by a two-step method; (d)-(f): Recovery results by proposed algorithm; (g)-(i) proposed algorithm with regularization

6. J. Rodenburg, A. Hurst, A. Cullis, B. Dobson, F. Pfeiffer, O. Bunk, C. David, K. Jefimovs, and I. Johnson, "Hard-x-ray lensless imaging of extended objects," *Phys. review letters* **98**, 034801 (2007).
7. M. Beckers, T. Senkbeil, T. Gorniak, M. Reese, K. Giewekemeyer, S.-C. Gleber, T. Salditt, and A. Rosenhahn, "Chemical contrast in soft x-ray ptychography," *Phys. Rev. Lett.* **107**, 208101 (2011).
8. A. Maiden, G. Morrison, B. Kaulich, A. Gianoncelli, and J. Rodenburg, "Soft x-ray spectromicroscopy using ptychography with randomly phased illumination," *Nat. communications* **4**, 1669 (2013).
9. R. Hoppe, J. Reinhardt, G. Hofmann, J. Patommel, J.-D. Grunwaldt, C. D. Damsgaard, G. Wellenreuther, G. Falkenberg, and C. Schroer, "High-resolution chemical imaging of gold nanoparticles using hard x-ray ptychography," *Appl. Phys. Lett.* **102**, 203104 (2013).
10. D. A. Shapiro, Y.-S. Yu, T. Tyliszczak, J. Cabana, R. Celestre, W. Chao, K. Kaznatcheev, A. D. Kilcoyne, F. Maia, S. Marchesini *et al.*, "Chemical composition mapping with nanometre resolution by soft x-ray microscopy," *Nat. Photonics* **8**, 765–769 (2014).
11. M. Farmand, R. Celestre, P. Denes, A. D. Kilcoyne, S. Marchesini, H. Padmore, T. Tyliszczak, T. Warwick, X. Shi, J. Lee *et al.*, "Near-edge x-ray refraction fine structure microscopy," *Appl. Phys. Lett.* **110**, 063101 (2017).
12. X. Shi, P. Fischer, V. Neu, D. Elefant, J. Lee, D. Shapiro, M. Farmand, T. Tyliszczak, H.-W. Shiu, S. Marchesini *et al.*, "Soft x-ray ptychography studies of nanoscale magnetic and structural correlations in thin smco5 films," *Appl. Phys. Lett.* **108**, 094103 (2016).
13. M. Lerotic, C. Jacobsen, T. Schäfer, and S. Vogt, "Cluster analysis of soft x-ray spectromicroscopy data," *Ultramicroscopy* **100**, 35–57 (2004).

Table 1. SNRs for results with different scan stepsizes by the two-step method, and proposed SPA without and with regularization.

stepsize		36	38	40
SNR	two-step	12.0	7.20	3.6
	SPA($\delta = 0$)	15.0	15.2	11.7
	SPA	15.8	15.9	13.5

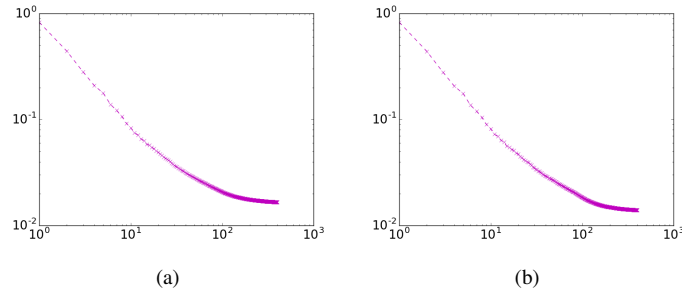


Fig. 6. Error $\frac{\|x^k - X^{k-1}\|}{\|X^k\|}$ changes v.s. iteration number for SPA without regularization in (a) and with regularization in (b)

14. Y.-S. Yu, M. Farmand, C. Kim, Y. Liu, C. P. Grey, F. C. Strobridge, T. Tyliszczak, R. Celestre, P. Denes, J. Joseph *et al.*, “Three-dimensional localization of nanoscale battery reactions using soft x-ray tomography,” *Nat. communications* **9**, 921 (2018).
15. V. Elser, “Phase retrieval by iterated projections,” *JOSA A* **20**, 40–55 (2003).
16. A. M. Maiden and J. M. Rodenburg, “An improved ptychographical phase retrieval algorithm for diffractive imaging,” *Ultramicroscopy* **109**, 1256–1262 (2009).
17. P. Thibault, M. Dierolf, O. Bunk, A. Menzel, and F. Pfeiffer, “Probe retrieval in ptychographic coherent diffractive imaging,” *Ultramicroscopy* **109**, 338–343 (2009).
18. P. Thibault and M. Guizar-Sicairos, “Maximum-likelihood refinement for coherent diffractive imaging,” *New J. Phys.* **14**, 063004 (2012).
19. Z. Wen, C. Yang, X. Liu, and S. Marchesini, “Alternating direction methods for classical and ptychographic phase retrieval,” *Inverse Probl.* **28**, 115010 (2012).
20. S. Marchesini, A. Schirotzek, C. Yang, H.-t. Wu, and F. Maia, “Augmented projections for ptychographic imaging,” *Inverse Probl.* **29**, 115009 (2013).
21. R. Horstmeyer, R. Y. Chen, X. Ou, B. Ames, J. A. Tropp, and C. Yang, “Solving ptychography with a convex relaxation,” *New journal physics* **17**, 053044 (2015).
22. R. Hesse, D. R. Luke, S. Sabach, and M. K. Tam, “Proximal heterogeneous block implicit-explicit method and application to blind ptychographic diffraction imaging,” *SIAM J. on Imaging Sci.* **8**, 426–457 (2015).
23. M. Odstrčil, A. Menzel, and M. Guizar-Sicairos, “Iterative least-squares solver for generalized maximum-likelihood ptychography,” *Opt. Express* **26**, 3108–3123 (2018).
24. H. Chang, P. Enfedaque, and S. Marchesini, “Blind ptychographic phase retrieval via convergent alternating direction method of multipliers,” *SIAM J. Imaging Sci.* **12**, 153–185 (2019).
25. J. B. Adams, M. O. Smith, and P. E. Johnson, “Spectral mixture modeling: A new analysis of rock and soil types at the viking lander 1 site,” *J. Geophys. Res. Solid Earth* **91**, 8098–8112 (1986).
26. N. Vaswani, S. Nayer, and Y. C. Eldar, “Low-rank phase retrieval,” *IEEE Transactions on Signal Process.* **65**, 4059–4074 (2017).
27. K. Liu, J. Wang, Z. Xing, L. Yang, and J. Fang, “Low-rank phase retrieval via variational bayesian learning,” *IEEE Access* **7**, 5642–5648 (2019).
28. Z. Chen, G. Jagatap, S. Nayer, C. Hegde, and N. Vaswani, “Low rank fourier ptychography,” in *2018 IEEE International Conference on Acoustics, Speech and Signal Processing (ICASSP)*, (IEEE, 2018), pp. 6538–6542.
29. R. Glowinski and P. Le Tallec, *Augmented Lagrangian and operator-splitting methods in nonlinear mechanics* (Philadelphia, PA: SIAM, 1989).

30. L. I. Rudin, S. Osher, and E. Fatemi, "Nonlinear total variation based noise removal algorithms," *Phys. D: Nonlinear Phenom.* **60**, 259–268 (1992).
31. H. Chang, Y. Lou, Y. Duan, and S. Marchesini, "Total variation–based phase retrieval for poisson noise removal," *SIAM J. on Imaging Sci.* **11**, 24–55 (2018).
32. H. Chang, P. Enfedaque, and S. Marchesini, "Iterative joint ptychography-tomography with total variation regularization," arXiv preprint arXiv:1902.05647 (2019).
33. S. Aslan, V. Nikitin, D. J. Ching, T. Bicer, S. Leyffer, and D. Gürsoy, "Joint ptycho-tomography reconstruction through alternating direction method of multipliers," *Opt. Express* **27**, 9128–9143 (2019).
34. C. Wu, J. Zhang, and X.-C. Tai, "Augmented lagrangian method for total variation restoration with non-quadratic fidelity," *Inverse problems imaging* **5**, 237–261 (2011).
35. A. Chambolle and T. Pock, "A first-order primal-dual algorithm for convex problems with applications to imaging," *J. mathematical imaging vision* **40**, 120–145 (2011).
36. H. Yan, C. Wang, A. R. McCarn, and H. Ade, "Accurate and facile determination of the index of refraction of organic thin films near the carbon 1 s absorption edge," *Phys. review letters* **110**, 177401 (2013).
37. R. d. L. Kronig, "On the theory of dispersion of x-rays," *Josa* **12**, 547–557 (1926).
38. M. Hirose, K. Shimomura, N. Burdet, and Y. Takahashi, "Use of kramers–kronig relation in phase retrieval calculation in x-ray spectro-ptychography," *Opt. express* **25**, 8593–8603 (2017).